Comp. Meth. Civil Eng., Vol.4 No.1 (2013) 1-24

CMCE

Computational Methods in Civil Engineering

Invited Paper

Buckling of functionally graded stiffened and unstiffened plates using finite strip method

S. Sarrami-Foroushani[a], M. Azhari [a,*], M. M. Saadatpour[a]

[a]*Department of Civil Engineering, Isfahan University of Technology, Isfahan,84156-83111, Iran*

Received 1 February 2014

Abstract

This paper deals with local buckling analysis of rectangular functionally graded material plates using finite strip method and based on classical plate theory. The modulus of elasticity of the plate is assumed to vary according to a power-law distribution in terms of the volume fractions of the constituents. The principle of minimum total potential energy is employed to obtain stiffness and stability matrices of functionally graded plate while a matrix eigenvalue problem is then solved to find the critical stresses of rectangular plates subjected to various types of loading including uniform and non-uniform uniaxial loadings and biaxial uniform loading. The accuracy of the proposed model is validated in which the obtained results are compared with those reported elsewhere. Furthermore, a comprehensive parametric study is performed to investigate the effects of various parameters such as boundary conditions, power law index, aspect ratio and type of loading on the local buckling coefficient of functionally graded material plates whilst the developed finite strip method is also employed to study the buckling behaviour of long stiffened functionally graded plates subjected to uniform uniaxial loading.

Keywords**:** Functionally graded material; Local buckling; Stiffened plates; Finite strip method

1. Introduction

New composite materials have been increasingly developed during last decades. Functionally graded materials (FGMs) were first introduced in Japan in 1984 [1]. FGMs are known as advanced high-performance and heat resistant materials which are able to withstand against ultra-high temperatures and extremely large thermal gradients that are usually developed in spacecrafts and nuclear plants. FGMs are microscopically inhomogeneous materials in which the mechanical and thermal properties vary smoothly and continuously from one surface to the other surface through the thickness. This is achieved by gradually varying the volume fraction of the constituent materials [2].

Buckling behaviour is one of the most important phenomena in the design of structural components such as plates. The buckling of rectangular functionally graded material plates has been investigated during last decades. Reddy [3] presented a finite element formulation for linear and nonlinear thermo-mechanical response of FGM plates employing higher order shear deformation theory. Vel and Batra [4] found an exact solution for the thermoelastic

[*]Corresponding author.
Tel.: +98 311 3913804. Fax: +98 311 3912700.
E-mail address: mojtaba@cc.iut.ac.ir

deformation of FGM thick rectangular simply supported plates. Suitable temperature and displacement functions that identically satisfied boundary conditions at the edges were used to reduce the partial differential equations governing the thermo-mechanical deformations to a set of coupled ordinary differential equations in the thickness coordinate, which were then solved by employing the power series method while the effective material properties at a point were estimated by either the Mori-Tanaka or the self-consistent schemes. Javaheri and Eslami [5, 6] investigated the buckling of the fully simply supported FGM plates subjected to uniform in-plane compressive and thermal loads using variational approach which was based on classical plate theory. They employed equilibrium and stability relationships to study the buckling behaviour of fully simply supported functionally graded material plates while thermal buckling of FGM plates was reported in the other research work using higher order shear deformation plate theory [7]. Buckling analysis of fully simply supported rectangular thick functionally graded plates under mechanical and thermal loads was presented by Samsam Shariat and Eslami [8] where it was assumed that the plate was under three types of mechanical loadings including uniaxial compression, biaxial compression, and biaxial compression and tension as well as two types of thermal loadings including uniform temperature rise and non-linear temperature rise through the thickness. The equilibrium and stability equations were derived using the third order shear deformation plate theory. The effect of imperfection on the buckling load of fully simply supported FGM plates subjected to in-plane compressive and thermal loadings was taken into consideration in the other studies using the classic plate theory [9-11].

The mechanical and thermal buckling analysis of functionally graded ceramic-metal plates with arbitrary geometry was presented by Zhao *et al*. [12] in which the first-order shear deformation plate theory, in conjunction with the element-free *kp*-Ritz method, was employed. The displacement field was approximated in terms of a set of mesh-free kernel particle functions while the bending stiffness was evaluated using a stabilised conforming nodal integration technique, and the shear and membrane terms were computed using a direct nodal integration method to eliminate the shear locking effects of very thin plates. Bodaghi and Saidi [13] presented an analytical approach for buckling analysis of thick functionally graded rectangular plates with various boundary conditions in which the coupled governing stability equations of FGM plates were converted into two uncoupled partial differential equations in terms of transverse displacement and boundary layer function. The Levy-type solution was employed to solve these equations for functionally graded rectangular plates with two opposite edges simply supported. Hoang and Nguyen [14] presented a simple analytical approach for the stability of functionally graded plates under in-plane compressive, thermal and combined loads. Equilibrium and compatibility equations for functionally graded plates were derived by using the classical plate theory taking into account both geometrical nonlinearity in von Karman sense and initial geometrical imperfection whilst the resulting equations were solved by Galerkin procedure to obtain explicit expressions of post-buckling load-deflection curves.

This paper addresses the buckling behaviour of rectangular functionally graded plates using finite strip method (FSM). In comparison to other numerical methods such as finite element method, the FSM, which was first introduced by Cheung [15], provides more efficient formulations for investigation of plate buckling behaviour under different load conditions. Ghannadpour and his colleagues used the FSM to investigate the buckling of rectangular functionally graded plates under three types of mechanical loadings, namely; uniaxial compression, biaxial compression, and biaxial compression and tension [16]. These authors also investigated thermal buckling of functionally graded plates using FSM [17]. Recently, the second author investigated mechanical buckling and free vibration of thick functionally graded plates resting on elastic foundation using the higher order B-spline finite strip method

[18]. However, hitherto its direct application to the local buckling behaviour of rectangular stiffened functionally grade material plates has not been investigated. Consequently the semi-analytical finite strip method is employed in this paper to investigate the buckling behaviour of FGM plates subjected to uniform and non-uniform uniaxial compressive loading, and uniform biaxial loading under different boundary conditions. Moreover, the presented methodology is used to study the local buckling of longitudinally stiffened functionally graded plates subjected to uniform uniaxial loadings.

2. Theory

2.1 Material modelling

FGMs are composed of a mixture of ceramic and metal or a combination of different metals by gradually varying the volume fraction of the constituent materials. In order to obtain the effective mechanical and thermal properties of FGM plate, a simple rule of mixture based on power-law distribution is assumed for which the material properties vary through the thickness of the plate as

$$P(z) = P_m + (P_c - P_m)V \ , \tag{1}$$

where subscripts *m* and *c* refer to the metal and ceramic constituents, respectively, *P* denotes a property of the material and *z* is measured over the thickness of the plate. In Eq.(1), *V* is the volume fraction of ceramic phase and is expressed by a power-law distribution such that

$$V = \left(\frac{z}{h} + \frac{1}{2}\right)^n , \tag{2}$$

in which *h* is the thickness of the plate, *n* is the power law index which is always positive and *z* is measured from the geometric centroid of the plate in which $-(h/2) \leq z \leq +(h/2)$. Figure 1 shows the variation of ceramic volume fraction through the thickness of the plate for different volume fraction exponents. It can be seen that the plate is fully ceramic when $n = 0$ while the composition of ceramic and metal takes a linear shape when $n = 1$.

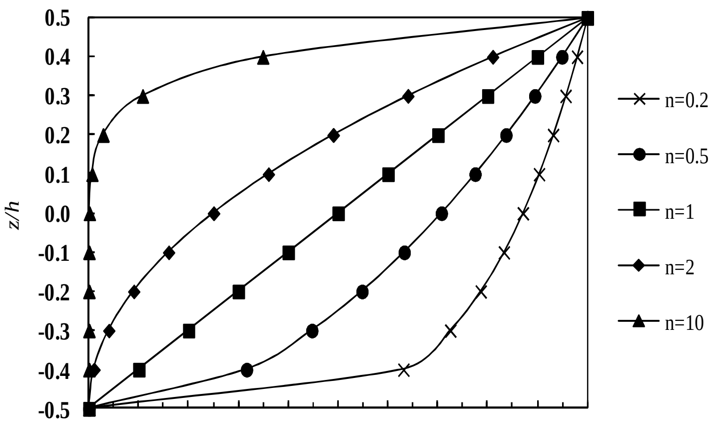

Figure 1. Variation of volume fraction over the thickness for different values of power index *n*

2.2 Differential equations of functionally graded plates

A rectangular element of a thin flat plate is depicted in Figure 2.

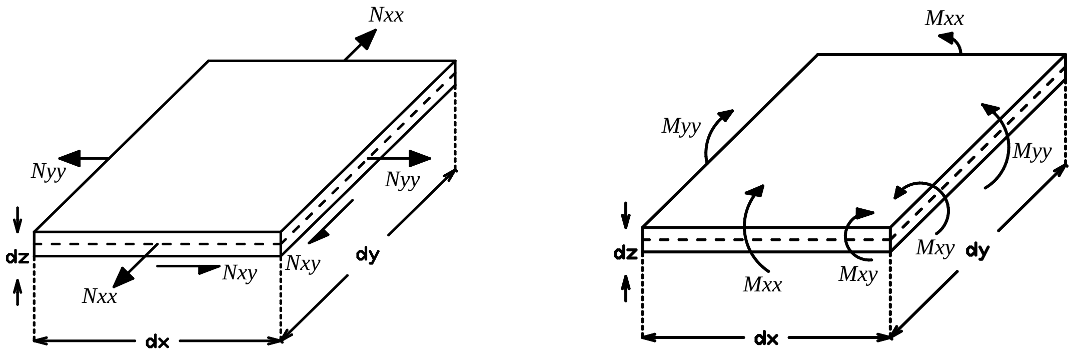

Figure 2. Internal forces and moments of the plate element

The in-plane forces and moments are also shown in this figure. According to the classical plate theory (CPT), the following equilibrium equations are expressed for homogeneous plates [5],

$$\frac{\partial N_{xx}}{\partial x}+\frac{\partial N_{yx}}{\partial y}=0 \ , \tag{3}$$

$$\frac{\partial N_{xy}}{\partial x}+\frac{\partial N_{yy}}{\partial y}=0 \ , \tag{4}$$

$$\frac{\partial^2 M_{xx}}{\partial x^2}+2\frac{\partial^2 M_{xy}}{\partial x\partial y}+\frac{\partial^2 M_{yy}}{\partial y^2}=-p_z-N_{xx}\frac{\partial^2 w}{\partial x^2}-2N_{xy}\frac{\partial^2 w}{\partial x\partial y}-N_{yy}\frac{\partial^2 w}{\partial y^2} \ , \tag{5}$$

where N_{xx}, N_{yy}, and N_{xy} are in-plane edge loads, M_{xx} and M_{yy} are bending moments about *x* and *y* axes, respectively, M_{xy} is the twisting moment, p_z is the external lateral load and *w* is lateral displacement of the mid-plane of the plate. The magnitude of the in-plane forces and moments can be obtained from

$$N_{ij}=\int_{-h/2}^{h/2}\sigma_{ij}\,\mathrm{dz} \qquad ; \qquad i,j=x,y \tag{6}$$

$$M_{ij}=\int_{-h/2}^{h/2}\sigma_{ij}\,\mathrm{zdz} \qquad ; \qquad i,j=x,y \tag{7}$$

It is worth noting that unlike homogeneous plates where the set of three equations (3) to (5) are not coupled and could be treated independently, for functionally graded plates these equations are coupled due to inhomogeneous behaviour of the material and should be solved simultaneously.
The relationship between the stresses and strains may be expressed as

$$\begin{Bmatrix}\sigma_{xx}\\ \sigma_{yy}\\ \tau_{xy}\end{Bmatrix}=\frac{E(z)}{1-\nu^2}\begin{bmatrix}1 & \nu & 0\\ \nu & 1 & 0\\ 0 & 0 & \frac{1-\nu}{2}\end{bmatrix}\begin{Bmatrix}\varepsilon_{xx}\\ \varepsilon_{yy}\\ \gamma_{xy}\end{Bmatrix} \tag{8}$$

in which $E(z)$ is the modulus of elasticity of the FGM plate which is determined by power law distribution given in Eq.(1) and ν is the Poisson's ratio which is assumed to be constant for both materials [5-9]. According to CPT, the displacement field at an arbitrary point is expressed by

$$u(x,y,z)=u(x,y)-z\frac{\partial w}{\partial x},\ v(x,y,z)=v(x,y)-z\frac{\partial w}{\partial y},\ w(x,y,z)=w(x,y) \tag{9}$$

The nonlinear strain-displacement relations, taking into account large rotations with small strains, are determined from

$$\begin{Bmatrix}\varepsilon_{xx}\\ \varepsilon_{yy}\\ \gamma_{xy}\end{Bmatrix}=\begin{Bmatrix}\dfrac{\partial u}{\partial x}+\dfrac{1}{2}\left(\dfrac{\partial w}{\partial x}\right)^2\\ \dfrac{\partial v}{\partial y}+\dfrac{1}{2}\left(\dfrac{\partial w}{\partial y}\right)^2\\ \dfrac{\partial u}{\partial y}+\dfrac{\partial v}{\partial x}+\dfrac{\partial w}{\partial x}.\dfrac{\partial w}{\partial y}\end{Bmatrix}-z\begin{Bmatrix}\dfrac{\partial^2 w}{\partial x^2}\\ \dfrac{\partial^2 w}{\partial y^2}\\ 2\dfrac{\partial^2 w}{\partial x\partial y}\end{Bmatrix} \tag{10}$$

Substituting Eq. (10) into Eqs. (6) to (8) leads to the in-plane forces N_{ij} and in-plane moments M_{ij} to be expressed as a function of displacement components. Equations (3) to (5) can be then manipulated such that the differential equation of FGM plate is derived as

$$\overline{D}\nabla^2\nabla^2 w(x,y)=p_z(x,y)+N_{xx}\frac{\partial^2 w}{\partial x^2}+2N_{xy}\frac{\partial^2 w}{\partial x\partial y}+N_{yy}\frac{\partial^2 w}{\partial y^2} \tag{11}$$

which resembles the governing differential equation of homogeneous plate subjected to distributed lateral load $p_z(x, y)$ as well as in-plane loads N_{xx}, N_{xy} and N_{yy} acting on the middle surface of the plate. In Eq.(11) ∇^2 is two-dimensional Laplacian operator, and

$$\overline{D}=\frac{I_1I_3-I_2^2}{I_1(1-\nu^2)} \tag{12}$$

in which

$$I_1=E_m h+\left(E_c-E_m\right)\left(\frac{h}{h+1}\right), \tag{13}$$

$$I_2=\left(E_c-E_m\right)h^2\left(\frac{1}{n+2}-\frac{1}{2n+2}\right) \tag{14}$$

$$I_3=E_m\frac{h^3}{12}+\left(E_c-E_m\right)h^3\left(\frac{1}{n+3}-\frac{1}{n+2}+\frac{1}{4n+4}\right), \tag{15}$$

where E_c and E_m are modulus of elasticity of ceramic and metal, respectively.

2.3 Solution procedure

The finite strip method, which is a well-known semi-analytical method, is employed in this section to investigate the buckling behaviour of rectangular functionally graded plates with different boundary conditions subjected to various types of in-plane compressive loading. Figure 3a shows a single strip in rectangular coordinate system (X, Y, Z) with two nodal lines *i* and *j* whilst the strip nodal degrees of freedom are shown in Figure 3b.

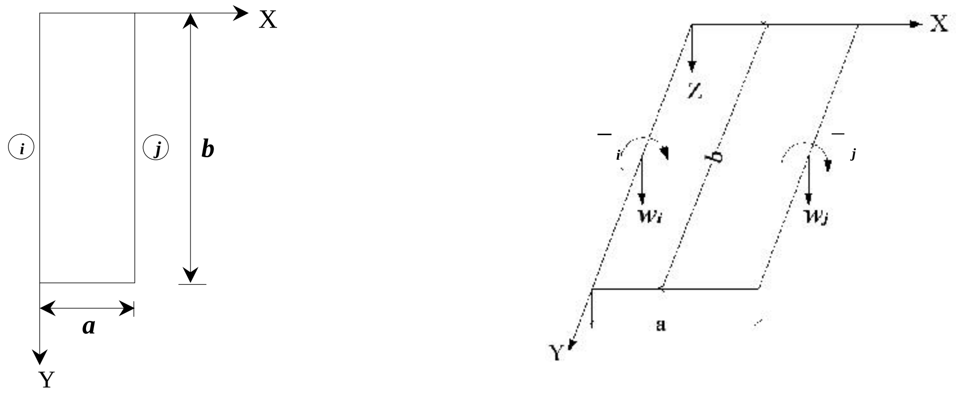

(a) (b)

Figure 3. A typical strip and degrees of freedom on its nodal lines

The deflection of the strip is defined as

$$w(x,y)=\sum_{q=1}^{r}X_q(x).Y_q(y), \tag{16}$$

in which r is number of harmonic modes, $X_q(x)$ is appropriate Hermitian shape function and $Y_q(y)$ is q^{th} mode of a trigonometric function and which are given in the Appendix.
Using Hermitian shape functions Eq. (16) may be written as

$$\begin{aligned} w(x,y)=\sum_{q=1}^{r}\Big[&(1-3\xi^2+2\xi^3)w_i^q+a(\xi-2\xi^2+\xi^3)\theta_i^q \\ &+(3\xi^2-2\xi^3)w_j^q+a(-\xi^2+\xi^3)\theta_j^q\Big]Y_n(y)\ ;\ \xi=x/a \end{aligned} \tag{17}$$

in which $\xi=x/a$, a is width of the strip and w_i^q, w_j^q, θ_i^q and θ_j^q are deflections and rotations of each nodal line corresponding to q^{th} mode as shown in Figure 3b. Eq.(17) can then be expressed in a vector form as

$$w(x,y)=\sum_{q=1}^{r}\mathbf{N}_q\boldsymbol{\delta}_q \tag{18}$$

where

$$\mathbf{N}_q=\left[1-3\xi^2+2\xi^3\quad a\left(\xi-2\xi^2+\xi^3\right)\quad 3\xi^2-2\xi^3\quad a\left(-\xi^2+\xi^3\right)\right]Y_q(y) \tag{19}$$

and δ_q , which is the displacement vector δ_q related to mode q, is given by

$$\boldsymbol{\delta}_q = \{w_i \quad \theta_i \quad w_j \quad \theta_j\}_q^{\mathrm{T}} = \begin{Bmatrix} \boldsymbol{\delta}_i^q \\ \boldsymbol{\delta}_j^q \end{Bmatrix} \tag{20}$$

in which $\theta_i = \left(\dfrac{\partial w}{\partial x}\right)_i$ and $\theta_j = \left(\dfrac{\partial w}{\partial x}\right)_j$. The total displacement vector of a strip with nodal lines i and j is then written as

$$\begin{Bmatrix} \boldsymbol{\delta}_i \\ \boldsymbol{\delta}_j \end{Bmatrix} = \sum_{q=1}^{r} \{w_i \quad \theta_i \quad w_j \quad \theta_j\}_q^{\mathrm{T}} Y_q(y) \tag{21}$$

The plate curvature vector, $\boldsymbol{\kappa}$, is derived by appropriate differentiation of displacement field given by Eq. (18) so that

$$\boldsymbol{\kappa} = \{\chi_x \quad \chi_y \quad 2\chi_{xy}\} = \left\{ -\frac{\partial^2 w}{\partial x^2} \quad -\frac{\partial^2 w}{\partial y^2} \quad -2\frac{\partial^2 w}{\partial x \partial y} \right\} \tag{22}$$

which can be written in a matrix form by substituting Eq.(18) into Eq.(22) such that

$$\boldsymbol{\kappa} = \sum_{q=1}^{r} \mathbf{B}_q \boldsymbol{\delta}_q = \mathbf{B}\boldsymbol{\delta} \tag{23}$$

in which $\boldsymbol{\delta}$ and $\mathbf{B}$ are total displacement vector and curvature matrix of the strip respectively, and $\mathbf{B}_q$ is curvature matrix corresponding to mode q which is given by

$$\mathbf{B}_q = \begin{bmatrix} -\dfrac{1}{a^2}(-6+12\eta)Y_q & -\dfrac{1}{a}(-4+6\eta)Y_q & -\dfrac{1}{a^2}(6-12\eta)Y_q & -\dfrac{1}{a}(-2+6\eta)Y_q \\ -(1-3\eta^2+2\eta^3)Y_q'' & -a(\eta-2\eta^2+\eta^3)Y_q'' & -(-3\eta^2-2\eta^3)Y_q'' & -a(-\eta^2+\eta^3)Y_q'' \\ -\dfrac{2}{a}(6\eta+6\eta^2)Y_q' & -2(1-4\eta+3\eta^2)Y_q'' & -\dfrac{2}{a}(6\eta-6\eta^2)Y_q' & -2(-2\eta+3\eta^2)Y_q' \end{bmatrix} \tag{24}$$

where Y_q' and Y_q'' are the first and second derivatives of Y_q with respect to y, respectively. The plate moment-curvature relationship is obtained from

$$\mathbf{M} = \mathbf{D}\boldsymbol{\kappa} \tag{25}$$

in which

$$\mathbf{M} = \{M_{xx} \quad M_{yy} \quad M_{xy}\} \tag{26}$$

and

$$\mathbf{D}=\overline{D}\begin{bmatrix} 1 & \neg & 0 \\ \neg & 1 & 0 \\ 0 & 0 & \frac{1-\neg}{2} \end{bmatrix} \tag{27}$$

The principle of minimum total potential energy is employed to find the stiffness and stability matrices of a typical strip. Strain energy of a strip, U, is defined as

$$U=\frac{1}{2}\int_0^b\int_0^a \boldsymbol{\kappa}^{\mathrm{T}}\mathbf{M}\,\mathrm{d}x\mathrm{d}y \tag{28}$$

Substituting Eqs. (23) and (25) into Eq. (28) leads to the strain energy to be written in terms of displacement vector of the strip such that

$$U=\frac{1}{2}\int_0^b\int_0^a \boldsymbol{\delta}^{\mathrm{T}}\mathbf{B}^{\mathrm{T}}\mathbf{D}\mathbf{B}\boldsymbol{\delta}\,\mathrm{d}x\mathrm{d}y \tag{29}$$

The work done W due to in plane stresses acting on the edges of the strip shown in Figure 4 is determined by

$$W=-\int_0^b\int_0^a £_N^T\,\boldsymbol{\sigma}\,\mathrm{d}x\mathrm{d}y \tag{30}$$

where $£_N$ is the nonlinear part of membrane strains and is given by

$$£_N=\left\{\frac{1}{2}\left(\frac{\partial w}{\partial x}\right)^2 \quad \frac{1}{2}\left(\frac{\partial w}{\partial y}\right)^2 \quad \frac{\partial w}{\partial x}.\frac{\partial w}{\partial y}\right\} \tag{31}$$

and the stress vector, $\boldsymbol{\sigma}$, is defined as

$$\boldsymbol{\sigma}=\{\pm_x \quad \pm_y \quad ²_{xy}\} \tag{32}$$

in which $\pm_x$, $\pm_y$ and $²_{xy}$ act on the boundaries of the plate as shown in Figure 4.

Substituting Eqs. (18) and (19) into Eq. (31) leads to $£_N$ to be expressed as

$$\boldsymbol{\varepsilon}_N=\left\{\sum_{q=1}^{r}\frac{1}{2}\boldsymbol{\delta}_q^{\mathrm{T}}\mathbf{S}_{qx}^{\mathrm{T}}\mathbf{S}_{qx}\boldsymbol{\delta}_q \quad \sum_{q=1}^{r}\frac{1}{2}\boldsymbol{\delta}_q^{\mathrm{T}}\mathbf{S}_{qy}^{\mathrm{T}}\mathbf{S}_{qy}\boldsymbol{\delta}_q \quad \sum_{q=1}^{r}\boldsymbol{\delta}_q^{\mathrm{T}}\mathbf{S}_{qx}^{\mathrm{T}}\mathbf{S}_{qy}\boldsymbol{\delta}_q\right\} \tag{33}$$

or

$$\boldsymbol{\varepsilon}_N=\left\{\frac{1}{2}\boldsymbol{\delta}^{\mathrm{T}}\mathbf{S}_x^{\mathrm{T}}\mathbf{S}_x\boldsymbol{\delta} \quad \frac{1}{2}\boldsymbol{\delta}^{\mathrm{T}}\mathbf{S}_y^{\mathrm{T}}\mathbf{S}_y\boldsymbol{\delta} \quad \boldsymbol{\delta}^{\mathrm{T}}\mathbf{S}_x^{\mathrm{T}}\mathbf{S}_y\boldsymbol{\delta}\right\} \tag{34}$$

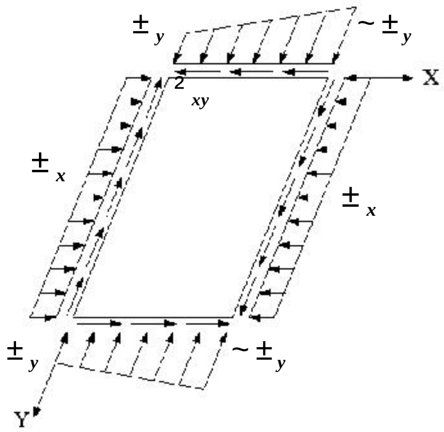

Figure 4. A typical strip subjected to bi-axial compression and shear loading

in which $\mathbf{S}_{qx}$ and $\mathbf{S}_{qy}$ are obtained from

$$\mathbf{S}_{qx} = \left[\frac{1}{a}\left(-6\P + 6\P^{2}\right) \quad 1-4\P+3\P^{2} \quad \frac{1}{a}\left(6\P - 6\P^{2}\right) \quad -2\P+3\P^{2} \right] Y_{q} \tag{35}$$

and

$$\mathbf{S}_{qy} = \left[1-3\P^{2}+2\P^{3} \quad a\left(\P-2\P^{2}+\P^{3}\right) \quad 3\P^{2}-2\P^{3} \quad a\left(-\P^{2}+\P^{3}\right) \right] Y_{q}' \tag{36}$$

The total potential energy stored in the elastic body of the strip can be written as

$$\Pi = U + W \tag{37}$$

Substituting Eqs.(29) and (30) into Eq.(37) with minimising Π respect to the displacement vector ¢ leads to

$$¢\Pi = 0 \Rightarrow \int_{0}^{b}\int_{0}^{a} \mathbf{B}^{\mathrm{T}}\mathbf{D}\mathbf{B}\boldsymbol{\delta}\,\mathrm{d}x\mathrm{d}y - \int_{0}^{b}\int_{0}^{a} \mathbf{B}_{qs}^{\mathrm{T}}\boldsymbol{\sigma}'\mathbf{B}_{qs}\boldsymbol{\delta}\,\mathrm{d}x\mathrm{d}y = \mathbf{0} \tag{38}$$

where

$$\mathbf{B}_{qs} = \begin{Bmatrix} \mathbf{S}_{qx} \\ \mathbf{S}_{qy} \end{Bmatrix} \tag{39}$$

and

$$\boldsymbol{\sigma}' = \begin{bmatrix} \pm_{x} & 2_{xy} \\ 2_{xy} & \pm_{y} \end{bmatrix}. \tag{40}$$

Equation (38) could be rearranged as

$$(\mathbf{K}-\mathbf{K}_G)\boldsymbol{\delta}=\mathbf{0} \tag{41}$$

in which $\boldsymbol{\delta}$ is the eigenvector and $\mathbf{K}$ and $\mathbf{K}_G$ are the global stiffness and stability matrices of the functionally grade plate, respectively, which are formed by assembling the stiffness and stability matrices of the strips, $\mathbf{K}^e$ and $\mathbf{K}_G^e$, using equilibrium and compatibility equations along nodal lines in which

$$\mathbf{K}_G^e=\mathbf{K}_{G,x}^e+\mathbf{K}_{G,y}^e+\mathbf{K}_{G,xy}^e \tag{42}$$

where the square sub-matrices of $\mathbf{K}_{G,x}^e$, $\mathbf{K}_{G,y}^e$ and $\mathbf{K}_{G,xy}^e$ can be written in the matrix form as

$$\left(\mathbf{K}_{G,x}^e\right)_{ij}=\int_0^b\int_0^a \mathbf{S}_{yi}^{\mathrm{T}}\pm_x\mathbf{S}_{yj}\,\mathrm{d}x\mathrm{d}y\ , \tag{43}$$

$$\left(\mathbf{K}_{G,y}^e\right)_{ij}=\int_0^b\int_0^a \mathbf{S}_{xi}^{\mathrm{T}}\pm_y\mathbf{S}_{xj}\,\mathrm{d}x\mathrm{d}y \tag{44}$$

and

$$\left(\mathbf{K}_{G,xy}^e\right)_{ij}=\int_0^b\int_0^a \mathbf{S}_{xi}^{\mathrm{T}}2\ {}_{xy}\mathbf{S}_{yj}\,\mathrm{d}x\mathrm{d}y\ . \tag{45}$$

Similarly, the square sub-matrices of the stiffness matrix $\mathbf{K}^e$ can be given by

$$\mathbf{K}_{ij}^e=\int_0^b\int_0^a \mathbf{B}_i^{\mathrm{T}}\mathbf{D}\mathbf{B}_j\,\mathrm{d}x\mathrm{d}y\ . \tag{46}$$

The buckling equation can be finally formulated as

$$\left|\mathbf{K}-\mathbf{K}_G\right|=0 \tag{47}$$

which is solved to obtain the critical buckling load.

3. Illustration

3.1 Verification

The accuracy of the proposed finite strip method in the previous section is investigated in this section and the obtained results are compared with those reported elsewhere. The local buckling coefficient, k, is defined as

$$k=\pm_{cr}\frac{12\left(1-\neg^2\right)(a/h)^2}{\circledR^2 E_m} \tag{48}$$

in which $\pm_{cr}$ is the critical buckling stress, v is the Poisson's ratio, E_m is the modulus of elasticity of the metallic surface of the plate, and a and h are the width and thickness of the FGM plate, respectively. The mechanical properties of the functionally graded materials are assumed to be E_c=380 GPa (for alumina), E_m=70 GPa (for aluminium) and ¬ =0.3.
Table 1 shows the magnitudes of the critical buckling stresses of the simply supported square FGM plates subjected to uniform uniaxial loading obtained from the proposed methodology in comparison to those reported by Shariat *et al*. [9]. It can be seen that the finite strip method developed in this paper can well describe the buckling behaviour of the simply supported square FGM plates for different values of power law index n.

Table 1. Critical buckling stresses (MPa) of FGM plates with SSSS boundary conditions given by proposed model in comparison to Ref. [9]

	n = 0	n = 1	n = 3	n = 10
Proposed model	137.388	68.479	48.636	41.161
Shariat *et al*.'s model [9]	137.379	68.475	48.636	41.160

Table 1 shows that the magnitudes of critical stresses increase with the reduction of power law index n, which indicates that a fully alumina plate (n = 0) is less prone to buckle in comparison to a FGM plate.
Table 2 compares the magnitudes of the critical buckling stresses of the fully clamped square FGM plates determined from the proposed model with those given by Wu *et al*.'s analytical model in which finite double Chebyshev polynomials were employed [19]. To ensure that the plate is enough thin such that the buckling occurs in the elastic region of the material, the plate width to thickness ratio (a/h) was assumed to be 100. The results given by the proposed finite strip method for different numbers of harmonic modes r are in a good agreement with those given in the literature [19] as indicated in Table 2.

Table 2. Critical buckling stresses (MPa) of FGM plates with CCCC boundary conditions given by proposed model (FSM) in comparison to Ref.[19]

Method		n = 0	n = 1	n = 2	n = 5	$n = \infty$
FSM	5 strips, 1 mode	354.43	176.66	137.85	116.58	65.29
	5 strips, 3 mode	347.66	173.29	135.22	114.35	64.04
	5 strips, 5 mode	346.84	172.88	134.90	114.08	63.89
-	Wu et al.'s model [19]	348.0	175.4	136	115.3	-

While the present paper addresses the local buckling behaviour of FGM plates, the proposed formulations are enough generic such that they can be used to predict the local buckling coefficients of homogenous plates (n = 0). Table 3 shows the magnitudes of local buckling coefficients for rectangular homogenous plates with different aspect ratios subjected to uniform uniaxial loading obtained from the finite strip method proposed in this paper in comparison to those given in the literature [20]. It is worth noting that the plate was clamped along loaded edges, and could be simply supported- simply supported (SS), clamped-clamped (CC) or simply supported-clamped (SC) along both unloaded (longitudinal) edges. It can be seen that a good agreement is achieved while the maximum error is less than 2.5%, and consequently the accuracy of the developed model is validated.

3.2 Numerical study

A comprehensive numerical study is presented in this section using the finite strip formulations developed in Section 2 to investigate the elastic local buckling behaviour of rectangular functionally graded material plates. Unstiffened and stiffened Plates with different boundary conditions under uniform and non-uniform uniaxial loadings as well as under uniform biaxial loading are investigated.

Table 3. Local buckling coefficients of homogenous plates (n = 0) with clamped loaded edges given by proposed model (FSM) in comparison to Ref.[20]

b/a	Longitudinal edges boundary conditions						
	SS			CC			SC
	FSM	Exact Ref. [20]	Error %	FSM	Exact Ref. [20]	Error %	FSM
0.4	27.12	27.12	0	27.99	-	-	27.50
0.5	18.19	-	-	19.36	19.2	0.83	18.69
0.6	13.38	13.38	0	14.91	-	-	14.02
0.75	9.53	-	-	11.69	11.4	2.54	10.40
0.8	8.73	8.73	0	11.12	-	-	9.68
1.0	6.74	6.74	0	10.12	10.08	0.40	8.07
1.2	5.84	5.84	0	9.60	-	-	7.57
1.25	5.71	-	-	9.28	9.94	6.64	7.53
1.4	5.46	5.45	0.18	8.64	-	-	7.41
1.5	5.38	-	-	8.40	8.32	0.96	7.01
1.6	5.35	5.34	0.18	8.29	-	-	6.72
1.75	5.29	-	-	8.28	8.08	2.48	6.44
1.8	5.18	5.18	0	8.29	-	-	6.37
2.0	4.85	4.85	0	7.88	7.88	0	6.23
3.0	4.41	4.42	0.23	7.41	-	-	5.84

3.2.1 Unstiffened FGM plates subjected to uniform uniaxial compression

Figures 5 and 6 show the magnitudes of local buckling coefficient given by Eq. (48) for fully simply supported (SSSS) and fully clamped (CCCC) rectangular FGM plates, respectively, subjected to uniaxial uniform compression loading with different values of power law index n respect to the aspect ratio b/a.

It can be seen that the values of buckling stresses increase with the reduction of volume fraction exponent while higher values of local buckling coefficients are obtained for plates with fully clamped boundary conditions. Also, it can be seen that likewise the homogeneous plates, for a given value of n the magnitude of local buckling coefficient k does not significantly vary when aspect ratio b/a is greater than 2.5. A similar behaviour is observed when the boundary conditions along the longitudinal edges of the FGM plate are changed; however as depicted in Figures 7 and 8, FGM plates with simply supported loaded edges (SS) and simply supported-clamped unloaded edges (denoted as SC in Figure 7) are more prone to buckle than the plates with simply supported loaded edges (SS) and clamped-clamped unloaded edges (denoted as CC in Figure 8). Also Figures 5 to 8 indicate that the rate of variation of local buckling coefficient k with power law index n become less as power law index n increases. Furthermore, the accurate result of FGM plates tend to be less sensitive to the variation of aspect ratio with the increase of power law index n, as the magnitude of local buckling coefficient k becomes constant after lower values of b/a for higher values of n.

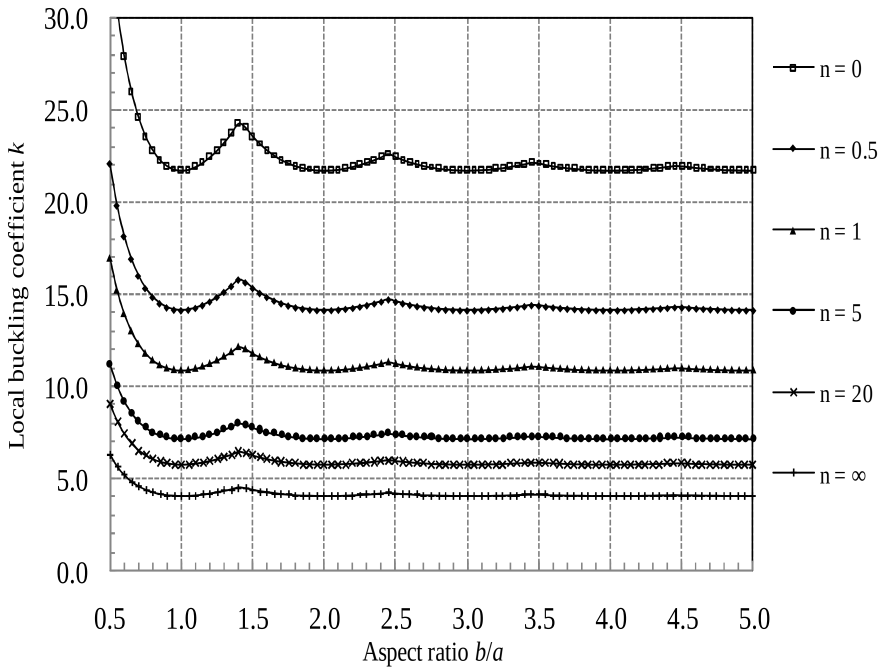

Figure 5. Local buckling coefficients of FGM plates with SSSS boundary conditions subjected to uniform uniaxial loading for different values of power law index *n*

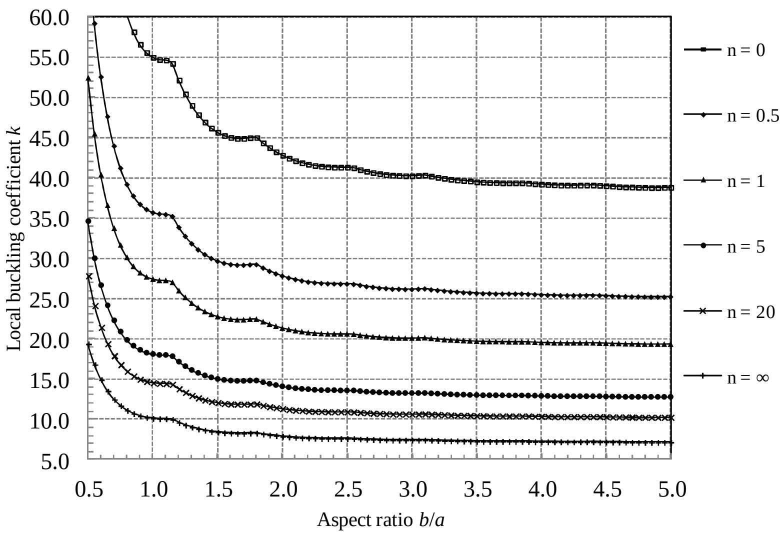

Figure 6. Local buckling coefficients of FGM plates with CCCC boundary conditions subjected to uniform uniaxial loading for different values of power law index *n*

The effect of asymmetric longitudinal boundary conditions on the value of local buckling coefficients of FGM plates with simply supported loaded edges under uniform uniaxial loading is depicted in Figure 9. The magnitude of power law index *n* is assumed to be unity. As expected, plates with higher rigidity along the longitudinal edges experience more values of local buckling coefficient; Furthermore, it can be seen that a FGM plate with clamped-guided longitudinal boundary condition (denoted as CG) needs four harmonic modes to get the accurate result when b/a = 5 while an accurate result is achieved by using only one mode for a FGM plate with simple supported-free longitudinal boundary conditions (denoted as SF).

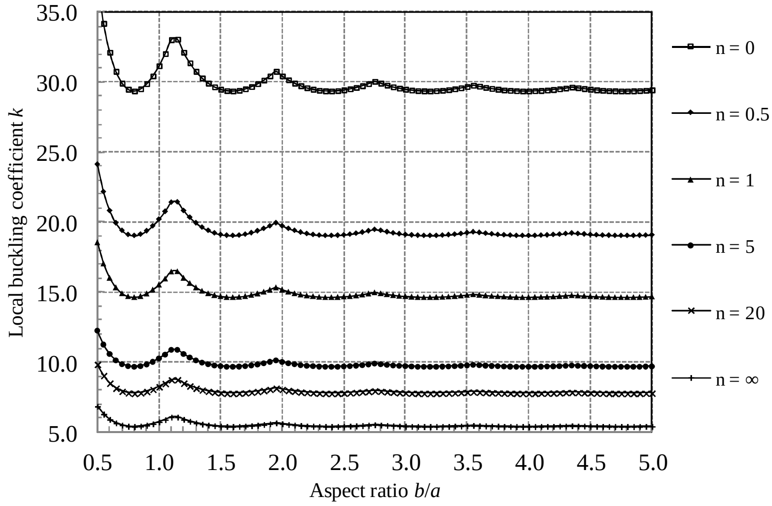

Figure 7. Local buckling coefficients of FGM plates with SSSC boundary conditions subjected to uniform uniaxial loading for different values of power law index n

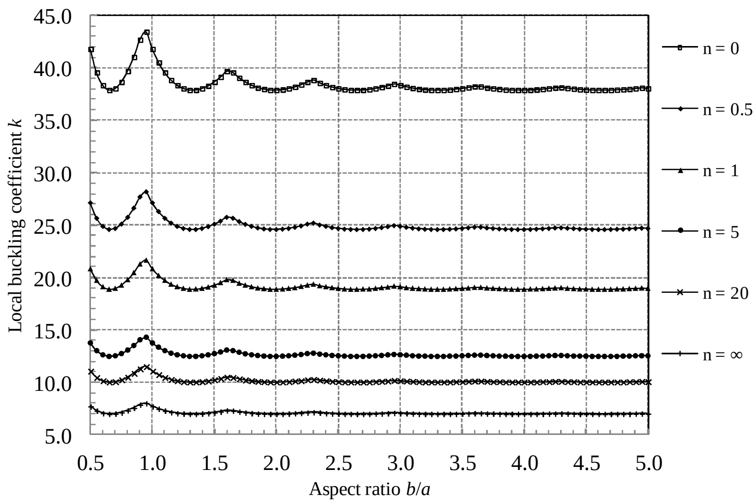

Figure 8. Local buckling coefficients of FGM plates with SSCC boundary conditions subjected to uniform uniaxial loading for different values of power law index n

It can be seen that the type of boundary conditions along the loaded edges of FGM plate is more significant for lower values of aspect ratio b/a for which regardless the loaded edges boundary conditions, the value of local buckling coefficient tends to a constant value at higher values of aspect ratio; however, the magnitude of this constant value depends significantly on the boundary conditions along unloaded (longitudinal) edges of the plate, and therefore plates with clamped-clamped (CC) unloaded edges experience higher values for local buckling coefficient (k = 18.886 when b/a > 5) than plates with simply supported-clamped (SC) or simply supported-simply supported (SS) unloaded edges (k = 14.644 and k = 10.824 for SC and SS plates, respectively) as depicted in Figures 11 and 12.

Figures 10 to 12 show the effect of the loaded edges boundary conditions on the magnitude of local buckling coefficient of FGM plates subjected to uniform uniaxial loading when the power law index is unity (n = 1).

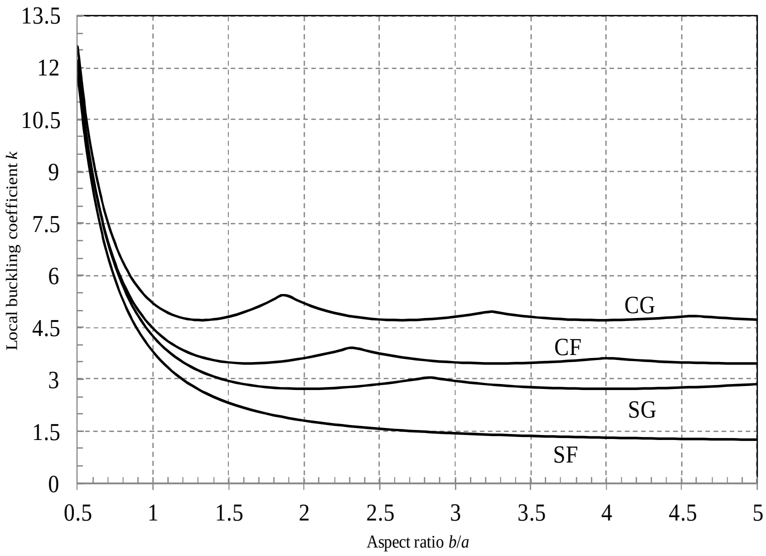

Figure 9. Local buckling coefficients of FGM plates (n = 1) with simply supported (SS) loaded edges subjected to uniform uniaxial loading.

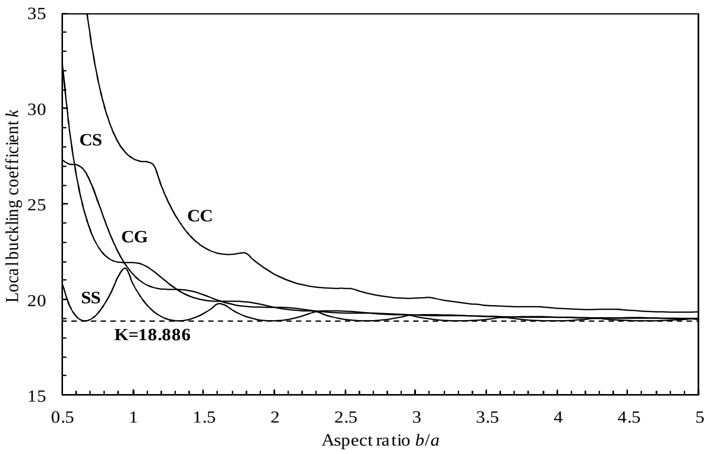

Figure 10. Local buckling coefficients of FGM plates (n = 1) with clamped-clamped (CC) longitudinal edges subjected to uniform uniaxial loading

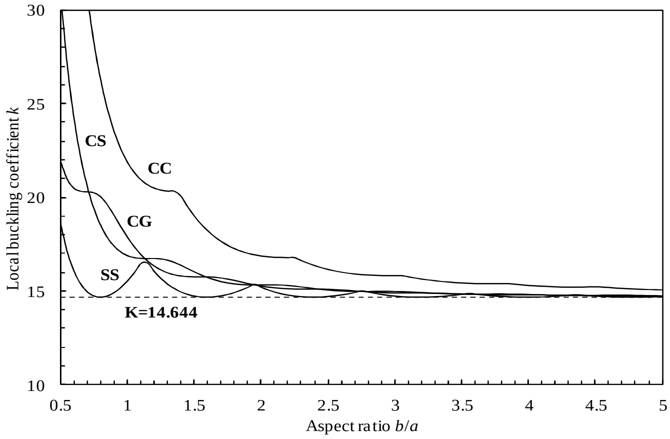

Figure 11. Local buckling coefficients of FGM plates (n = 1) with simply supported-clamped (SC) longitudinal edges subjected to uniform uniaxial loading

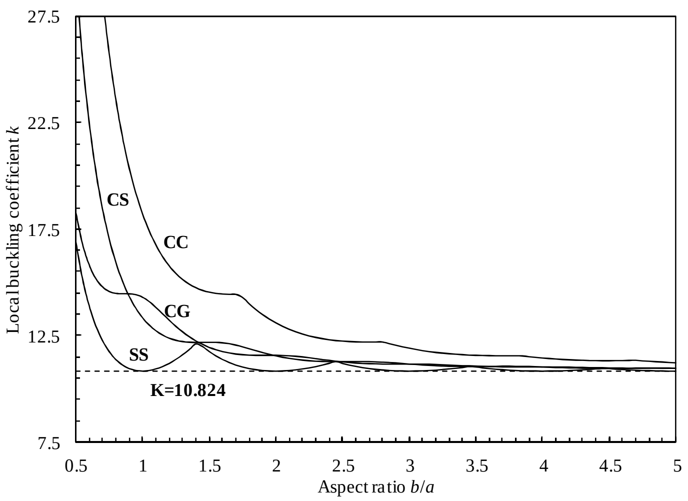

Figure 12. Local buckling coefficients of FGM plates (n = 1) with simply supported (SS) longitudinal edges subjected to uniform uniaxial loading

3.2.2 Unstiffened FGM plates subjected to non-uniform uniaxial compression

The buckling behaviour of functionally graded material plates subjected to non-uniform uniaxial loading is presented in this section in which FGM plates with different boundary conditions are taken into consideration. Figures 13a and b show FGM plates that are subjected to uniaxial triangular and pure bending loadings which are corresponding to ~== 0 and ~== -1 in Figure 4, respectively.

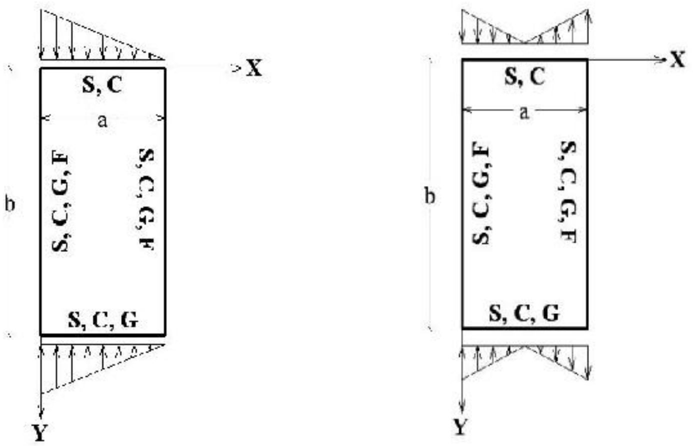

(a) (b)

Figure 13. Rectangular FGM plate subjected to (a) triangular loading (b) pure bending

The variations of the magnitudes of local buckling coefficients k with respect to aspect ratio b/a for a linear functionally grade material plates (n = 1) subjected to triangular loading (~ = 0) and bending moment (~ = -1) are shown in Figures 14 and 15 in which the longitudinal (unloaded) edges of FGM plate are assumed to be simply supported (SS) while the loaded edges can be SS, SC or CC. It can be seen that in the same manner to plates subjected to uniform uniaxial loading, the magnitude of local buckling coefficient is less sensitive to the type of loaded edges boundary conditions when the value of aspect ratio increases.

Likewise to homogenous plates, FGM plates subjected to uniform loading are more prone to buckle than plates subjected to triangular loading or pure bending, as depicted in Figure 16 for a fully simply supported FGM plate, which is due to the increase of the plate stiffness caused by tensile stresses when ~ = -1. Furthermore, FGM plates subjected to pure bending (~= -1) need more harmonic modes to achieve the accurate result as shown in Figure 16.

3.2.3 Unstiffened FGM plates subjected to uniform biaxial loading

The effect of uniform biaxial loading on the buckling behaviour of unstiffened rectangular FGM plates is investigated in this section. Figure 17a shows a FGM plate which is subjected to uniform biaxial compression loading of $_{1}\pm_{0y}$ and $_{2}\pm_{0x}$ in y and x directions respectively.

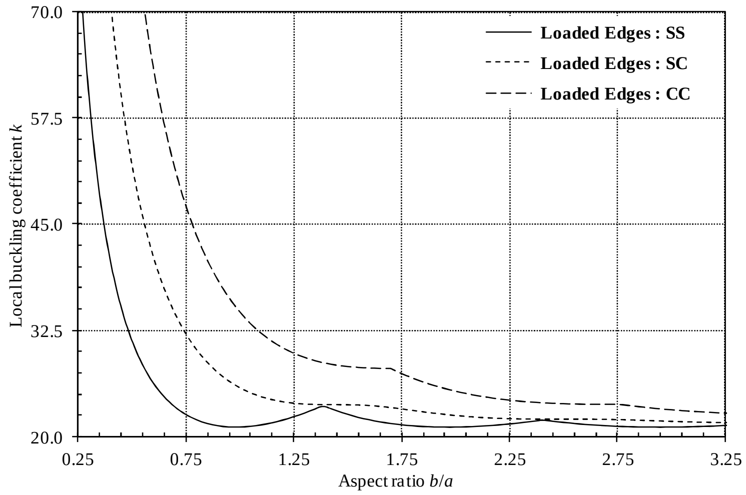

Figure 14. Local buckling coefficients of FGM plates (n = 1) with simply supported (SS) longitudinal edges subjected to triangular load

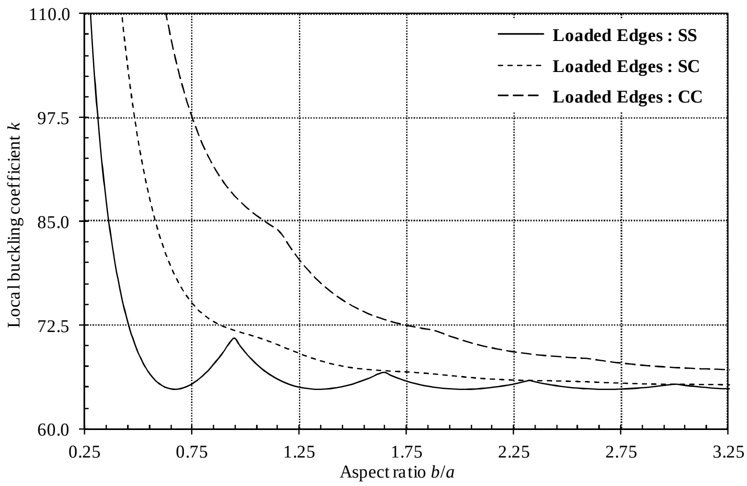

Figure 15. Local buckling coefficients of FGM plates (n = 1) with simply supported (SS) longitudinal edges subjected to pure bending

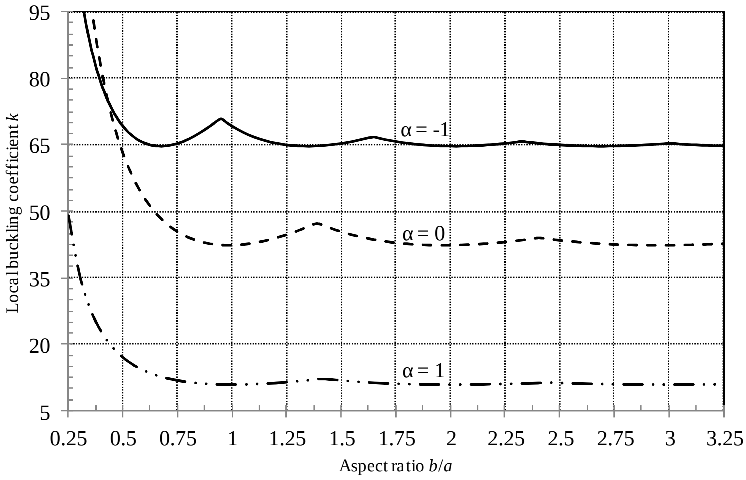

Figure 16. Local buckling coefficients of fully simply supported FGM plates (n = 1) under different types of uniaxial loading

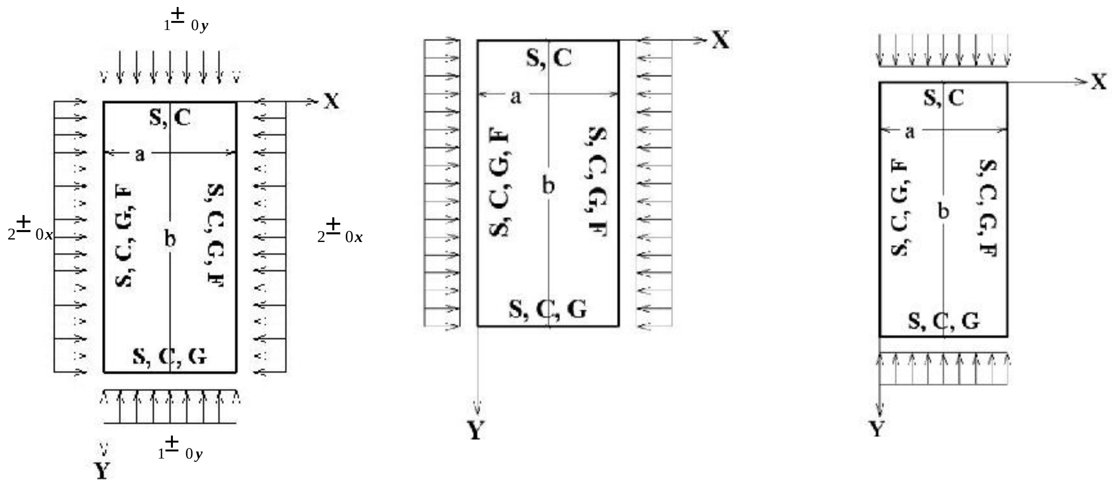

(a) (b) (c)

Figure 17. Rectangular FGM plate subjected to (a) biaxial loading (b) uniaxial uniform loading in x direction (c) uniaxial uniform loading in y direction

$\pm_{0y}$ and $\pm_{0x}$ are critical buckling stresses due to uniform uniaxial loading as depicted in Figure 17 b and c. It is worth noting that since there is two stability matrices $\mathbf{K}^{e}_{G,x}$ and $\mathbf{K}^{e}_{G,y}$, therefore one of them is assumed as a known matrix and the other one is calculated by using Eq.(47).

Figure 18 shows the interaction curves for fully simply supported FGM plates subjected to biaxial loading in which the ratio of width to thickness of plate (a/h) and the power law index (n) are assumed to be 100 and 1, respectively. Positive and negative signs indicate the compression and tension load cases, respectively.

As depicted in Figure 18, with a good approximation, $_1$ varies linearly respect to $_2$ when the aspect ratio b/a is greater than or equal to 2 and $_2 < 0$. The magnitudes of critical buckling stresses are shown in Table 4. It can be seen that for higher absolute values of $_2$, the magnitude of aspect ratio has more significant effect on the critical value of $_1$.

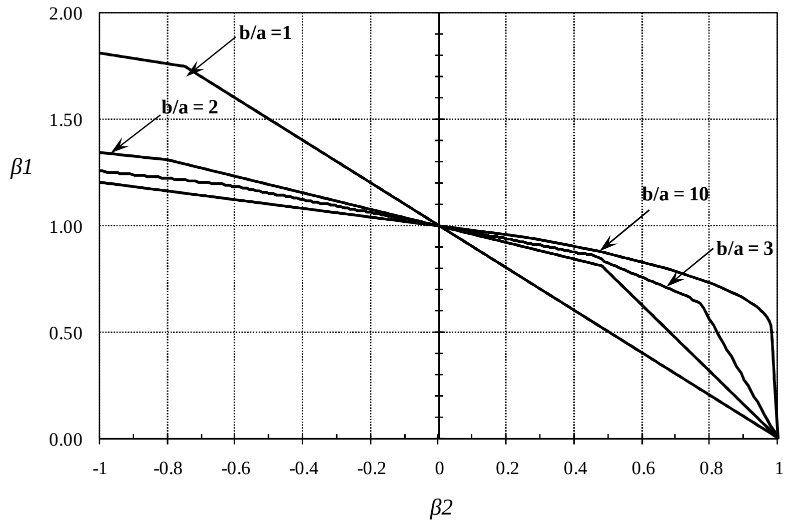

Figure 18. Interaction curves for FGM fully simply supported (SSSS) plate subjected to biaxial loading

Table 4. Critical buckling stresses of FGM plates (n = 1) with simply supported boundary conditions subjected to biaxial loading

b/a	$\pm_{0x}$ (MPa)	$\pm_{0y}$ (MPa)	2	1	$\pm_x$ (MPa)	$\pm_y$ (MPa)
1	68.477	68.477	-1	1.8124	-68.477	124.108
			-0.75	1.75	-51.358	119.835
			-0.5	1.5	-34.239	102.716
			-0.25	1.25	-17.119	85.596
			0.25	0.75	17.119	51.358
			0.5	0.5	34.239	34.239
			0.75	0.25	51.358	17.119
2	106.99	68.477	-1	1.3472	-106.99	92.252
			-0.75	1.293	-80.243	88.541
			-0.5	1.1953	-53.495	81.851
			-0.25	1.0977	-26.748	75.167
			0.25	0.9023	26.748	61.790
			0.5	0.78132	53.495	53.502
			0.75	0.3907	80.243	26.751
3	190.21	68.477	-1	1.2587	-190.21	86.192
			-0.75	1.2153	-142.658	83.22
			-0.5	1.1543	-95.105	79.043
			-0.25	1.0772	-47.553	73.763
			0.25	0.9228	47.553	63.191
			0.5	0.8264	95.105	56.589
			0.75	0.6528	142.658	44.702

3.2.4 Longitudinally stiffened plates under uniform uniaxial loading

The finite strip method developed in Section 2 is used in this section to investigate the buckling capacity of longitudinally stiffened long FGM plates shown in Figure 19 which are subjected to uniform uniaxial loading. As shown in Figure 19, the upper surface of the plate is made of ceramic while it continuously changes through the thickness of the plate to the metallic surface.

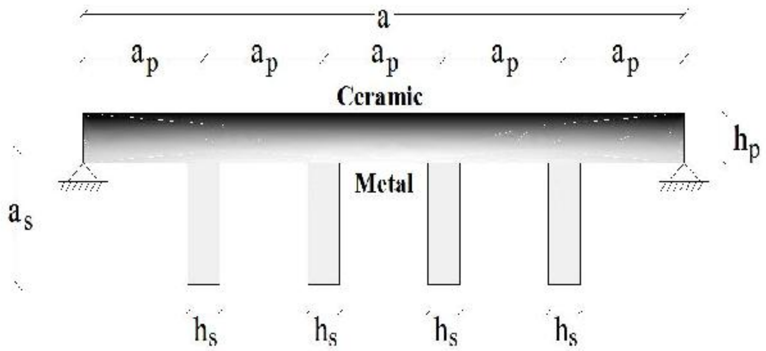

Figure. 19. Cross section of stiffened functionally graded material plate

It is assumed that the longitudinal stiffeners are made of the homogenous metallic material used at lower surface of FGM plate. The critical buckling stress σ_{cr} is obtained by using Eq.(47) whilst the local buckling coefficients of plate and stiffener (which are denoted as k_p and k_s respectively) are determined by

$$k_p = \sigma_{cr} \frac{12\left(1-\nu^2\right)\left(a_p / h_p\right)^2}{\pi^2 E_m} \tag{49}$$

$$k_s = \sigma_{cr} \frac{12\left(1-\nu^2\right)\left(a_s / h_s\right)^2}{\pi^2 E_m} \tag{50}$$

in which E_m is the modulus of elasticity of the FGM metallic surface, a_p and h_p are the width and thickness of the plate and a_s and h_s are the width and thickness of the stiffener, as shown in Figure 19.

Three buckling modes are considered; Mode I: local buckling of the plate between the stiffeners which occurs when the plate is reinforced by strong ribs; Mode II: local buckling of stiffeners, and Mode III: overall buckling of the plate-stiffener system. In order to determine the governing buckling mode, the ratio of the minimum half wave length to the width of plate (denoted as $L_{\min}/a_p$) as well as the ratio of the minimum half wave length to the width of the stiffener (denoted as $L_{\min}/a_s$) are calculated and compared with the corresponding ratios for the FGM plates with SSCC (simply supported loaded edges and clamped unloaded edges) and SSSS (simply supported loaded and unloaded edges) boundary conditions as well as with the corresponding ratios for homogenous plates (which represent the homogenous stiffeners) with SSCF and SSSF boundary conditions. Table 5 indicates the magnitudes of $L_{\min}/a$ and local buckling coefficients k for both stiffener (n = 0) and FGM plate which are given by Ref. [20] and Figures 5 and 8 respectively.

Tables 6 and 7 show the local buckling coefficients k_p and k_s for stiffened functionally graded material plates consisted of four equal plates with three stiffeners which are subjected to uniform uniaxial loads at both simply supported loaded edges while the power law index n is assumed to be 5 or ∞.

Table 5. Local buckling coefficients of long FGM and homogenous plates

		FGM section		Stiffener (Metallic)	
Boundaries		SSCC	SSSS	SSCF	SSSF
L_{min}/b:		0.64	1	1.65	∞
k	*n*= ∞	6.98	4		
	n=20	10.027	5.746		
	n=5	12.462	7.142	1.281	0.464
	n=1	18.886	10.824		
	n=0.5	24.562	14.076		

Table 6. Local buckling coefficients and buckling modes of stiffened FGM plates (*n* = 5)

h_s/h_p	b_s/b_p	$L_{\min}/b_p$	$L_{\min}/b_s$	K_p	K_s	Buckled
1/3	0.25	0.414	1.656	2.272	1.128	Stiffener
	0.5	0.824	1.648	0.568	1.277	Stiffener
	1	1.646	1.646	0.142	1.273	Stiffener
	1.5	2.466	1.644	0.063	1.274	Stiffener
1	0.25	1.01	4.04	7.185	0.449	Both
	0.5	1.044	2.088	4.161	1.040	Stiffener
	1	1.82	1.82	1.116	1.116	Stiffener
	1.5	2.652	1.768	0.510	1.147	Stiffener
2	0.25	0.828	3.312	9.392	0.147	Plate
	0.5	1.272	2.544	8.373	0.523	Both
	1	2.49	2.49	3.053	0.763	Stiffener
	1.5	3.44	2.293	1.470	0.827	Stiffener
3	0.25	0.804	3.216	9.596	0.067	Plate
	0.5	0.818	1.636	9.462	0.263	Plate
	1	3.24	3.24	5.476	0.609	Stiffener
	1.5	4.432	2.955	2.627	0.657	Stiffener

Table 7. Local buckling coefficients and buckling modes of stiffened FGM plates (*n* = ∞)

h_s/h_p	b_s/b_p	$L_{\min}/b_p$	$L_{\min}/b_s$	K_p	K_s	Buckled
1/3	0.25	0.428	1.712	2.197	1.236	Stiffener
	0.5	0.832	1.664	0.565	1.271	Stiffener
	1	1.656	1.656	0.141	1.268	Stiffener
	1.5	2.48	1.653	0.063	1.276	Stiffener
1	0.25	0.976	3.904	4.628	0.289	Plate
	0.5	1.184	2.368	3.280	0.820	Stiffener
	1	1.952	1.952	1.025	1.025	Stiffener
	1.5	2.7	1.8	0.498	1.121	Stiffener
2	0.25	0.812	3.248	5.336	0.083	Plate
	0.5	0.848	1.696	5.190	0.324	Plate
	1	2.801	2.801	2.698	0.674	Stiffener
	1.5	3.86	2.573	1.309	0.736	Stiffener
3	0.25	0.8	3.2	5.393	0.038	Plate
	0.5	0.808	1.616	5.355	0.149	Plate
	1	0.804	0.804	5.362	0.596	Plate
	1.5	0.8	0.533	5.363	1.341	Plate

It can be seen from Table 6 that when $h_s / h_p = 0.5$ and $a_s / a_p = 0.5$, the ratio of minimum half wave length to the width of the plate is $L_{\min} / a_p = 0.818$ which is between the values of 0.64 and 1 given in Table 5 corresponding to the FGM plate, and the ratio of minimum half wave length to the width of the stiffener is $L_{\min} / a_s = 1.636$ which is less than 1.65 given in Table 5 corresponding to the stiffener. Therefore the buckling mode is Mode I in which the plate buckles and the local buckling coefficient is 9.462 (which is between 12.462 and 7.142 given in Table 5). The comparison of Tables 6 and 7 indicates that when the magnitude of power law index *n* increases, Mode I in which the FGM plate between the stiffeners buckles, is more likely to occur which is due to the reduction of the stiffness of the FGM plate.

4. Conclusions

The buckling response of rectangular functionally graded plates was investigated using finite strip method in which the effect of different parameters such as volume fraction exponent, plate aspect ratio, loading type and boundary conditions on the buckling response of the plate was comprehensively studied. It was observed that the critical buckling load of functionally graded plate generally decreases with the increase of power law index. Moreover, the accurate results for plates with lower rigidity along the longitudinal edges of the plate are achieved by using less number of harmonic modes than plates with higher rigidity. It was also found that the type of boundary conditions along the loaded edges of FGM plate is more significant for lower values of aspect ratio *b*/*a* for which regardless the loaded edges boundary conditions, the value of local buckling coefficient tends to a constant value at higher values of aspect ratio.

Local buckling coefficients of long stiffened FGM plates were also obtained using the developed finite strip method. The effect of volume fraction exponent *n* and ratio of stiffener thickness to plate thickness on the buckling response was presented. It was observed that stiffened FGM plates are prone to buckle in three modes including buckling of FGM plate, buckling of stiffener and overall buckling of the plate-stiffener system. Furthermore it was found that when the power law index *n* increases, the FGM plate between the stiffeners is more prone to buckle which is due to the reduction of the stiffness of the FGM plate.

References

[1] Y. Miyamoto, *Functionally Graded Materials: Design, Processing, and Applications*, Kluwer Academic Publishers, 1999.

[2] M. Bouazza, A. Tounsi, E.A. Adda-Bedia, A. Megueni, Thermoelastic stability analysis of functionally graded plates: An analytical approach, *Computational Materials Science*, Vol. 49, (2010) 865-70.

[3] J.N. Reddy, Analysis of functionally graded plates, *International Journal for Numerical Methods in Engineering*, Vol. 47 (2000) 663-84.

[4] S.S. Vel, R.C. Barta, Exact Solution for Thermoelastic Deformations of Functionally Graded Thick Rectangular Plates, *AIAA Journal*, Vol. 40 (2002) 1421-33.

[5] R. Javaheri, M.R. Eslami, Buckling of functionally graded plates under in-plane compressive loading, *ZAMM Journal*, Vol. 82 (2002) 277-83.

[6] R. Javaheri, M.R. Eslami, Thermal buckling of functionally graded plates, *AIAA Journal*, Vol. 40 (2002) 162-9.

[7] R. Javaheri, M. R. Eslami, Thermal buckling of functionally graded plates based on higher order theory, *Journal of thermal stresses*, Vol. 25 (2002) 603-25.

[8] B.A. Samsam Shariat, M.R. Eslami, Buckling of thick functionally graded plates under mechanical and thermal loads, *Composite Structures*, Vol. 78 (2007) 433-9.

[9] B.A. Samsam Shariat, R. Javaheri, M. R. Eslami, Buckling of imperfect functionally graded plates under

in-plane compressive loading, *Thin-Walled Structures*, Vol. 43 (2005) 1020-36.

[10] B.A. Samsam Shariat, M.R. Eslami, Effect of initial imperfection on thermal buckling of functionally graded plates, *Journal of thermal stresses*, Vol. 28 (2005) 1183-98.

[11] B.A. Samsam Shariat, M.R. Eslami, Thermal buckling of imperfect functionally graded plates, *International Journal of Solids and Structures*, Vol. 43 (2006) 4082-96.

[12] X. Zhao, Y.Y. Lee, K.M. Liew, Mechanical and thermal buckling analysis of functionally graded plates, *Composite Structures*, Vol. 90 (2009) 161-71.

[13] M. Bodaghi, A.R. Saidi, Levy-type solution for buckling analysis of thick functionally graded rectangular plates based on the higher-order shear deformation plate theory, *Applied Mathematical Modelling*, Vol. 34 (2010) 3659–73.

[14] V.T. Hoang, D.D. Nguyen, Nonlinear analysis of stability for functionally graded plates under mechanical and thermal loads, *Composite Structures*, Vol. 92 (2010) 1184-91.

[15] Y.K. Cheung, The finite strip method in the analysis of elastic plates with two opposite simply supported ends, *Proc. Inst. Civ. Eng*, Vol. 40 (1968) 1–7.

[16] S.A.M. Ghannadpour, H.R. Ovesy, M. Nassirnia, An Investigation on Buckling Behaviour of Functionally Graded Plates Using Finite Strip Method, *Applied Mechanics and Materials*, Vol. 152-154 (2012) 1470-6.

[17] S.A.M. Ghannadpour, H.R. Ovesy, M. Nassirnia, Buckling analysis of functionally graded plates under thermal loadings using the finite strip method, *Computers and Structures* Vol. 108–109 (2012) 93–9.

[18] H. Foroughi, M. Azhari, Mechanical buckling and free vibration of thick functionally graded plates resting on elastic foundation using the higher order B-spline finite strip method, *to be published in Meccanica,* DOI 10.1007/s11012-013-9844-2.

[19] T.L. Wu, K.K. Shukla, J.H. Huang, Post-buckling analysis of functionally graded rectangular plates, *Composite Structures,* Vol. 81 (2007) 1-10.

[20] M.A. Bradford, M. Azhari, Buckling of Plates with Different End Conditions Using the Finite Strip Method, *Computers and Structuresm* Vol. 56 (1995) 75-83.

Appendix-A:

Type A1 of Trigonometric shape functions:

Boundary Condition	Shape Function
SS	$\sin\frac{m\pi y}{b}$
SC	$\sin\frac{(m+1)\pi y}{b}+\left(\frac{m+1}{m}\right)\sin\frac{m\pi y}{b}$
CC	$\sin\frac{m\pi y}{b}\sin\frac{\pi y}{b}$
CG	$\sin\frac{(m-1/2)\pi y}{b}\sin\frac{\pi y}{2b}$
CF	$1-\cos\frac{(m-1/2)\pi y}{b}$

Type A2 of Trigonometric shape functions:

Boundary Condition	Shape Function
SS	$\sin\frac{m\pi y}{b}$
SC	$J\left(\frac{\alpha_m y}{b}\right)-\frac{J(\alpha_m)}{H(\alpha_m)}H\left(\frac{\alpha_m y}{b}\right)$ $\alpha_m=\left(\frac{4m+1}{4}\right)\pi$
CC	$J\left(\frac{\alpha_m y}{b}\right)-\frac{J(\alpha_m)}{H(\alpha_m)}H\left(\frac{\alpha_m y}{b}\right)$ $\alpha_m=\left(\frac{2m+1}{2}\right)\pi$
CG	$J\left(\frac{\alpha_m y}{b}\right)-\frac{F(\alpha_m)}{J(\alpha_m)}H\left(\frac{\alpha_m y}{b}\right)$ $\alpha_m=\left(\frac{4m-1}{4}\right)\pi$
CF	$J\left(\frac{\alpha_m y}{b}\right)-\frac{G(\alpha_m)}{F(\alpha_m)}H\left(\frac{\alpha_m y}{b}\right)$ $\alpha_m=\left(\frac{2m-1}{2}\right)\pi$
SG	$\sin\frac{(2m-1)\pi y}{2b}$

in which

$F(u)=\sinh u+\sin u \qquad G(u)=\cosh u+\cos u$

$H(u)=\sinh u-\sin u \qquad J(u)=\cosh u-\cos u$

and

$$u = \frac{a_m y}{b}$$